Available online at www.sciencedirect.com

ScienceDirect

Procedia Manufacturing 47 (2020) 335–341

Procedia MANUFACTURING

www.elsevier.com/locate/procedia

23rd International Conference on Material Forming (ESAFORM 2020)

Insights in Strain and Stress States of Conical Shapes Flow Forming

Andrea Ghiotti[a,*], Michele Brun[a], Enrico Simonetto[a], Stefania Bruschi[a], Giorgio Muffato[b]

[a]*University of Padova, Department of Industrial Engineering, via Venezia 1, 35131, Padova, Italy*
[b]*Ronal AG, Lerchenbühl 3, 4624, Härkingen, Switzerland*

* Corresponding author. Tel.: +39 049 8276822; *E-mail address:* andrea.ghiotti@unipd.it

Abstract

Flow forming is an incremental forming process frequently used in manufacturing axi-symmetric parts that require high mechanical properties and fatigue resistance for dynamic applications, such as automotive and aerospace, or large-size components whose deformation in one step would require excessive loads. Nevertheless, the process design still remains challenging since the strain and stress states of the locally-deformed material are not clearly understood. To fill this gap, the paper focuses on the numerical modelling of forward flow forming, when it is applied to freeform-section profiles. The reference process is the flow forming of an aluminium alloy automotive wheel carried out in hot conditions. Results in terms of strains and stresses applied to the material by the rollers are presented, showing that relevant hydrostatic pressure conditions may be general with beneficial effects on the material formability.

Keywords: flow forming; AlSi7Mg; finite element method (FEM); forming;

1. Introduction

Flow forming has become a standard for the manufacturing of large size axi-symmetric parts that require high mechanical properties and fatigue resistance for dynamic applications thanks to the reduced forming loads and the possibility to obtain near-net-shape parts.

Over the years many researchers have investigated the main aspects of flow forming, with particular regard to the process mechanics, the influence of the process variables as well as the material response during deformation. The mechanics of the process was outlined in Wong et al. [1], discussing about the action of the main variables on the metal flow. They reported that the condition that allows having sound components happens when the circumferential contact length between the part and the roller is larger than the axial one: in such case the metal flow develops in axial direction, allowing the reduction in thickness and the consequent increase in the axial length of the workpiece.

To understand the deformative mechanism of flow forming process, Xu et al. [2] investigated the deformation state in flow forming thanks to a rigid-plastic FE model, summarizing the results in terms of principal stresses and strains. They classified the area near the contact region into three regions according to different deformations in axial, radial and circumferential directions. Hua et al. [3] developed an elasto-plastic FE model of three-rolled backward flow forming and present the strain history of two elements located respectively in outer and inner material thickness layer. The inner element is subjected to positive strains in the axial direction and negative strains in the radial direction, while the circumferential strains are lower with respect to the previous ones. Similar behavior was observed for the outer element, with the difference that the action of the roller generates redundant strains in both axial and radial directions, due to material build up in front of the roller. Recently, Mohebbi and Akbarzadeh [4], through experimental and numerical analyses, investigated the effect of the redundant strain during flow forming. They classified

10.1016/j.promfg.2020.04.270

the redundant strain into two components: a shear strain, occurring along the longitudinal and circumferential direction, and a radial strain that determined the material pile-up. The main effect of redundant strains is to increase the plastic equivalent strain without contribute to the final deformation.

Thanks to different experimental tests, Jahazi and Ebrahimi [5] presented an explanation about the connection between the contact areas ratio and the so-called attack angle for different values of the feed rate and they found that, for a given thickness reduction, the latter must not exceed a limit value in order to have a stable plastic flow. Wong et al. [6,7] studied the effect of the tool geometry on the material flow by using both flat and rounded-profile rollers. Davidson et al. [8] performed several tube spinning testes with different values of process parameters, considering rotation speed of the mandrel, roller feed rate and thickness reduction, in order to detect the optimal values of these parameters to maximize the final elongation of the workpiece. Ma et al. [9] simulated damage evolution in tube spinning and compared the accuracy of various damage fracture criteria to predict material failure. Xu et al. [10] simulated the damage evolution in tube spinning with six different damage fracture criteria and reported the influence of thinning rate on crack initiation.

However, despite the numerous researches and the efforts to understand the influence of process parameters on the response of flow formed material, the link between material properties and flow-formability is not yet clear. Bylya et al. [11] outlined a connection between the material flow-formability and the uniaxial elastic-plastic characteristics of the material, namely the resilience, the strain hardening and the reduction of area. In addition, the same Authors proposed a new experimental test to evaluate the attitude of the material to be deformed in multi-pass tube spinning. However, the experimental results were only qualitative and not fully representative of the material flow formability.

The aim of the present paper is to investigate the stress and strain state in the locally deformed material under the action of the rollers. To this aim, a FE model representative of automotive wheels hot flow forming was set up. The evolution of the stresses and strains was monitored by means of three numerical sensors and the main results are discussed.

2. Industrial case

Initial workpiece form (presented in Fig. 1), made of AlSi7Mg (Al – 7 wt % Si – 0.3 wt % Mg), is produced via low-pressure die casting process and subsequently heated up to the recrystallization temperature (390 °C). The hot workpiece is mounted in flow forming apparatus, where the action of three rollers determines the reduction in thickness and longitudinal elongation of the workpiece. After flow forming, workpiece dimensions and geometry are near at those ones of the final component. Table 1 shows geometric characteristics of the rollers normalized with respect to the roller diameter, and the main process conditions. The axial feed rate varies during process: initially, the rollers engaged the workpiece at low feed rate (3 mm/s – 5 mm/s) and, then, it increases linearly till the end of the stroke.

The three rollers are characterized by different values of nose radius. Therefore, as the value of the nose radius decrease, the material portion deformed by the roller becomes smaller. To better understand the local behavior of the deformed material, the stress and strain components under the smallest nose radius were analyzed by means of FE model of the industrial process.

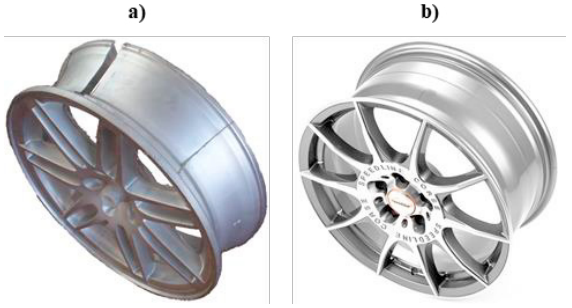

Fig. 1. a) Initial workpiece geometry; b) final component.

Table 1 – Rollers dimensions and process parameters

Parameter	Value
Rollers diameter	1
First roller nose radius	0.08
Second roller nose radius	0.05
Third roller nose radius	0.03
Mandrel speed	600 rpm
Average feed rate	10 mm/s

3. Numerical FE model

3.1. Numerical model set-up

The model set-up is presented in Fig. 2. The 3D numerical model was developed using the implicit software Transvalor Forge NXT 2.0™. The workpiece is considered as elasto-plastic model, numerically modeled by mean of Hansel-Spittel relation. Tools and mandrel were modeled as rigid body. To simulate the effect of the tailstock and the workpiece rotation, nodes at the head of the workpiece were constrained in z and θ directions. The former to reproduce the effect of the tailstock that keeps fixed the rims, the latter to simplify the contact condition at the interface between the mandrel and the wheel by imposing the spindle speed directly on the workpiece nodes. The workpiece is modelled with 9660 nodes and 51030 tetrahedral elements, with a maximum size of 7 mm, refined at 1.5 mm under the rollers. The process time implemented in the numerical simulation was 23 seconds, while the overall computation time is between one hundred and one hundred and ten hours.

The initial workpiece temperature is imposed equal to 390 °C, corresponding to the heating temperature of the workpiece in the industrial reference process.

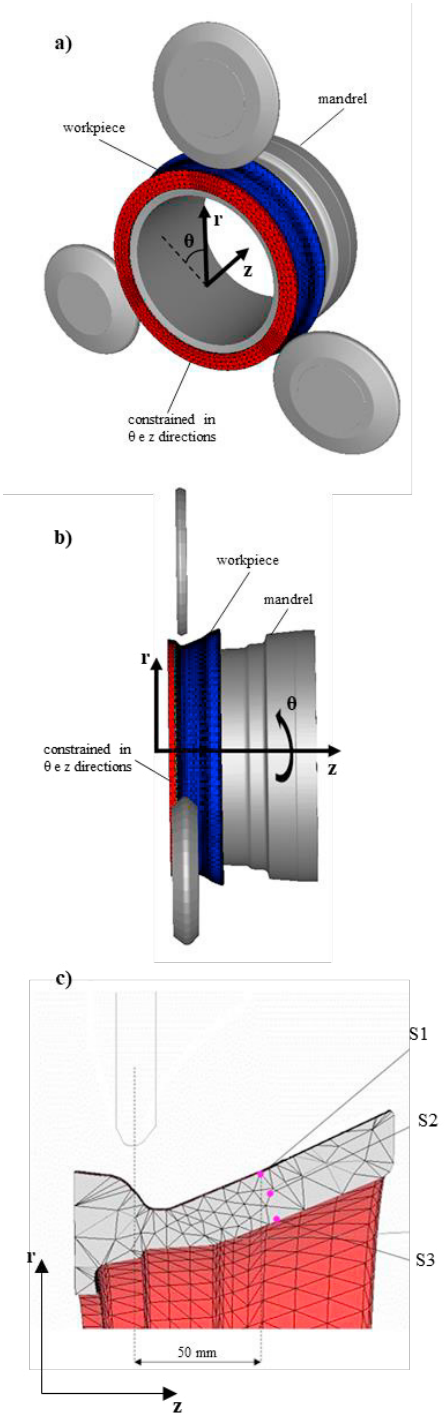

Fig. 2. FE model of flow forming process: a) prospective view; b) lateral view; c) numerical sensors applied at nodes mesh.

To study the evolution of the stresses and strains during the process, three sensors were applied to the mesh nodes. The numerical sensors were positioned at different radii to monitor the material behavior in different wheel layers: sensor 1 (S1) was indicative of the material at the outer surface of workpiece, sensor 2 (S2) was used for the intermediate layer, and sensor 3 (S3) for the material behavior at the inner workpiece surface.

3.2. Material model

The constitutive model of AlSi7Mg aluminium alloy implemented in the FE analysis was represented by the Hansel-Spittel equation, expressed as:

$$\sigma = Ae^{m_1 T} T^{m_9} \varepsilon^{m_2} e^{m_4/\varepsilon} (1+\varepsilon)^{m_5 T} e^{m_7} \dot{\varepsilon}^{m_3} \dot{\varepsilon}^{m_8 T} \quad (1)$$

where σ is the equivalent flow stress, ε the strain, $\dot{\varepsilon}$ the strain rate and T the temperature. The constitutive parameters (A, m_1, m_2, m_3, m_4, m_5, m_7, m_8, m_9) were calibrated by means of hot compression tests with the temperatures of 300 °C, 350 °C, 400 °C and strain rate values of 0.5 s^{-1}, 5 s^{-1}, 100 s^{-1}. The flow stress curves used for constitutive parameters calibration are reported in [12].

Table 2 – Hansel-Spittel constitutive parameters

Parameter	Value	Parameter	Value	Parameter	Value
A	143.205	m_3	0.0057	m_7	- 0.1706
m_1	- 0.0056	m_4	- 0.0012	m_8	0.0001
m_2	0.0403	m_5	0.0010	m_9	0.2692

4. Numerical results and discussion

4.1 Stress components and hydrostatic pressure

Since the roller geometry affects only a small portion of material, the first step of the analysis consisted in identifying the time interval of the numerical simulation in which each sensor is affected by the action of the roller. This has been done by identifying three temporal steps. In the first step, the sensor precedes the roller by a distance equal to the roller nose radius, in the second one the sensor is under the roller nose, and, finally, in the third step, the sensor is behind the roller, being at a distance from the roller equal to the value of the roller nose radius, as for the first step. Therefore, the first and last steps indicate the beginning and the end of the deformation.

Fig. 3, Fig. 4 and Fig. 5 present the relative position between the sensors and the roller and the plot of the stress tensor components vs. the time, referred to cylindrical coordinates system.

The stress components that are more affected by the action of the roller are normal stress in radial direction (σ_r), normal stress in axial direction (σ_z) and shear stress acting along radial-axial direction (τ_{rz}).

For the sensor 1 (S1), the radial and axial stresses initially assume respectively positive (tensile) and negative (compression) value, because the external layers of workpiece are compressed in axial direction and elongated in radial direction from the roller. This occurs to the outer material in front of the rollers, where the workpiece is more sensitive to the build-up. As S1 approaches the roller nose, the build-up is recovered and both the radial and axial stresses rapidly decrease down to negative values.

When S1 is below the roller nose, the radial and axial stresses assume the maximum compression values. After that, as the roller moves ahead from the material interested by S1, the radial and axial stresses decrease and reach positive values – in particular for the axial stress – due to the fact that the roller movement induces a tensile stress state on the material.

With respect to the radial-axial shear stress τ_{rz}, Fig. 3 shows an increase as the roller approaches, and a subsequent decrease when roller passes S1.

A similar trend is observable for sensor 2 (S2) from Fig. 4. The radial stress becomes negative (with compressive values) when the roller approaches S2 and reaches the maximum compressive value when S2 is under the nose radius. After that, as the roller moves axially, the compressive radial stresses gradually decrease. In the same way, the axial stress tends to negative values when the roller approaches S2 and grows to positive values when roller pass S2. Regarding the shear stress components, once again the only one affected by the action of the roller is the radial-axial stress.

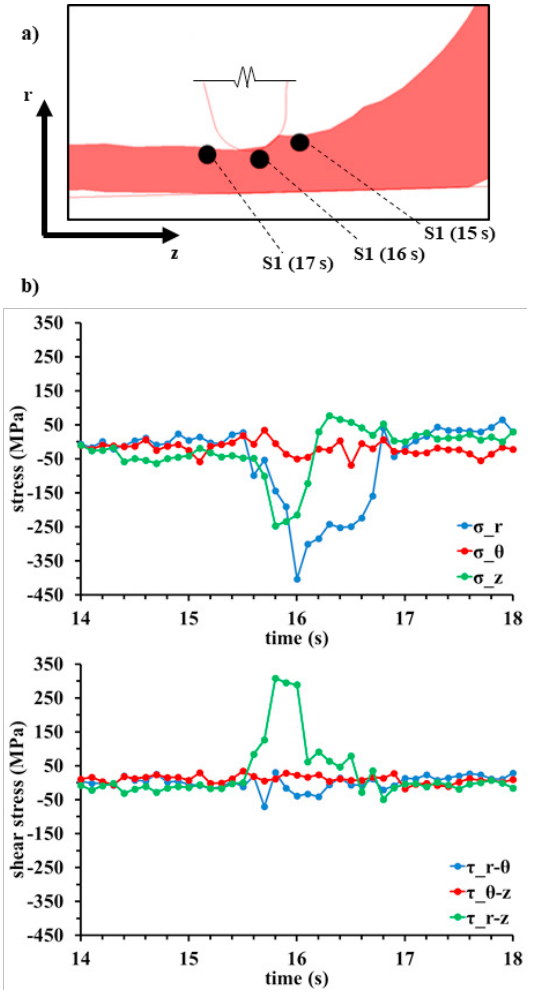

Fig. 3. a) relative position between sensor 1 (S1) and roller nose and corresponding time instants; b) stress tensor components for S1.

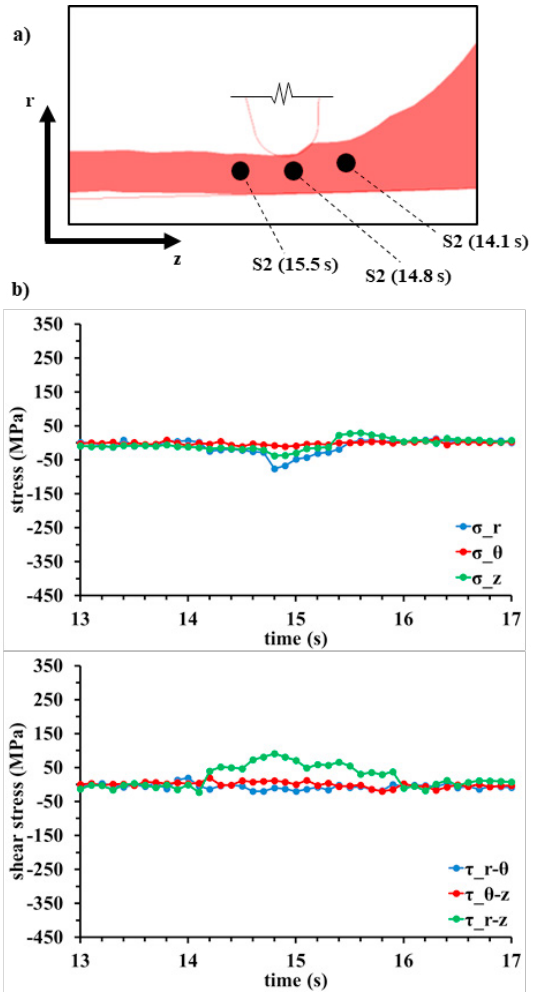

Fig. 4. a) relative position between sensor 2 (S2) and roller nose and corresponding time instants; b) stress tensor components for S2.

Fig. 5 shows the time step at which the sensor 3 (S3) is interested by the deformation and the evolution of the stress components in the corresponding time period.

In particular, the radial stress component is the only affected by the action of the roller, while the components in the axial and circumferential direction are almost negligible. The shear stress components are minimally influenced by the movement of the roller and during the deformation time their value ranges between -50 MPa and 50 MPa.

Fig. 6 shows the trends and the average values of the hydrostatic pressure as detected by the numerical sensors. When the three sensors are closed to the roller, the hydrostatic pressure assumes positive values (compression). The material of the workpiece locally deformed is subjected to a compressive state. The maximum hydrostatic pressure values are recorded by the three sensors when they are under the roller nose: in this region the maximum compression of the material occurs. Once the roller moves forward, the hydrostatic pressure becomes negative as the material is subjected to a tensile stress due to the effect of the increase axial tensile load and the decrease of radial compression. Despite the hydrostatic pressure assumes negative values

after the action of the roller, the average value during the deformation remains positive. S1 presents the maximum compression values because it is directly interested by the action of the roller. S2 average hydrostatic pressure value shows a marked decrease because both the radial and axial compressions decrease in respect of S1.

In the case of S3, the hydrostatic pressure average value increases due to the greater compression registered by radial and axial stress components and the low values assumed by shear stress components, as it is shown in Fig. 5.

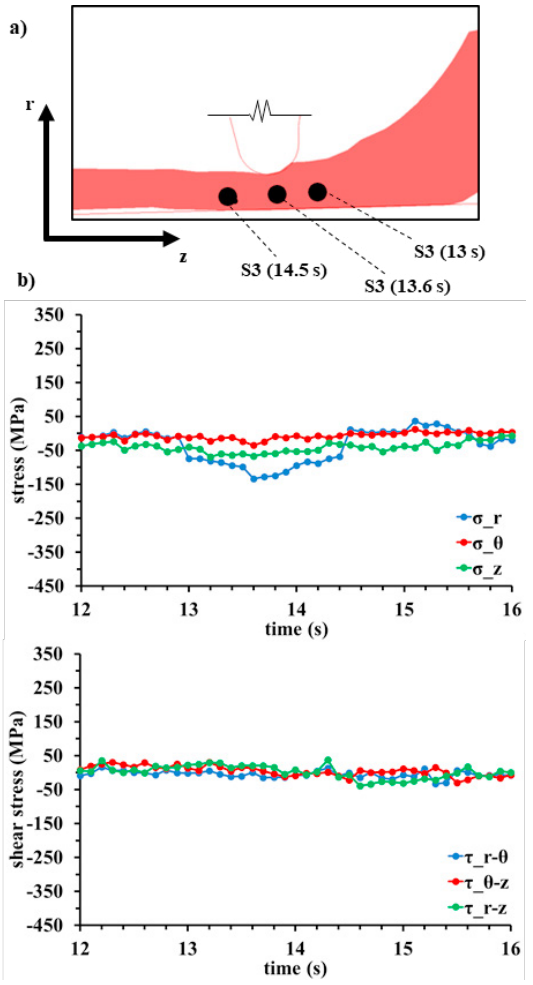

Fig. 5. a) relative position between sensor 3 (S3) and roller nose and corresponding time instants; b) stress tensor components for S3.

4.1. Strain components

In this section, the evolution of stain tensor components during the flow forming process are presented.

Radial strain trend (Fig. 7) shows that when the roller incoming, the material is pulled up and elongated in radial direction, while, once the roller has passed, the material is radially compressed. A gradient in radial strain along the thickness of workpiece exists and the amount of elongation and compression is more marked for the outer material layers (see S1).

Regarding circumferential components (Fig. 8), outer layers (see sensor S1) are subjected to positive strain that is equivalent to the material elongation in circumferential direction.

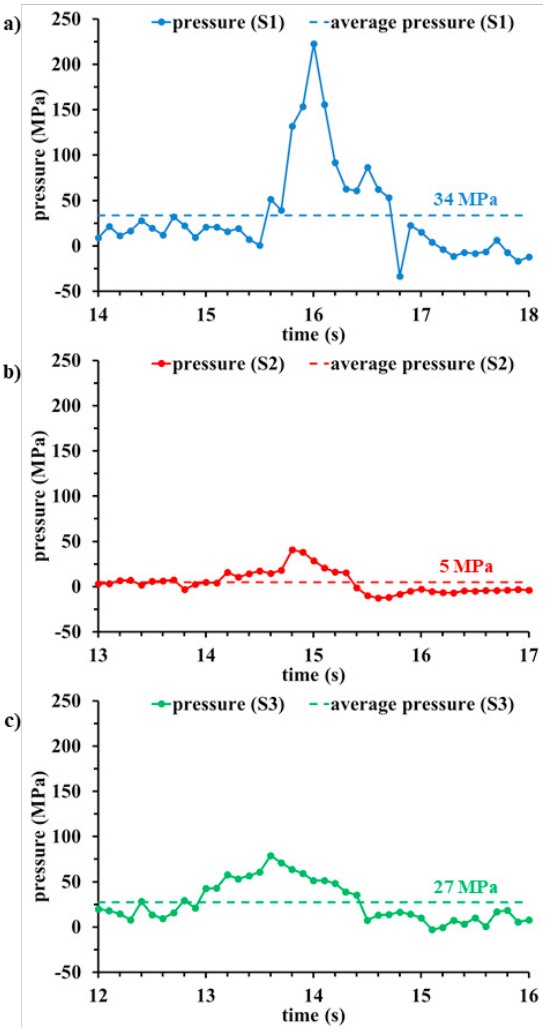

Fig 6. Hydrostatic pressure: a) sensor 1 (S1); b) sensor 2 (S2); c) sensor 3 (S3).

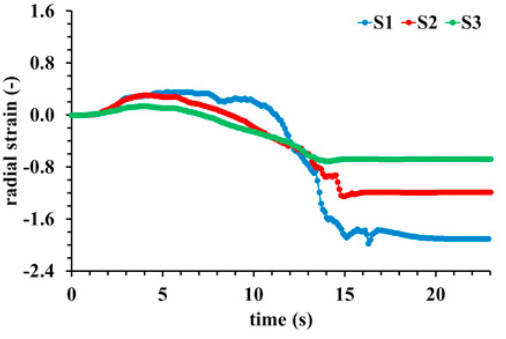

Fig. 7. Radial strain evolution during process time.

As shown in Fig. 9, the roller initially compresses the workpieces in axial direction and, then, material is elongated. The initial compression presents a thickness-dependent behavior, with higher values for outer layers (S1). Instead, the outer and the intermediate layers (S2) exhibit an axial tensile strain almost similar, both larger than the inner layers.

The radial-circumferential shear strain (reported in Fig. 10) represents the rotational sliding across the workpiece meridian section. Initially, the radial-circumferential shear strain of the outer layers (S1) and intermediate layers (S2) presents the same values: this means that these layers are sliding in counter-rotating direction with respect to the direction of rotation of the mandrel and workpiece. After the roller moves away from the material in which the sensors are attached, this strain is recovered.

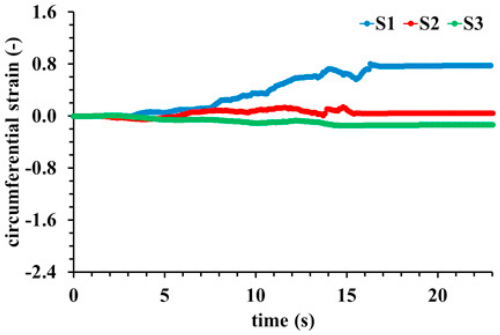

Fig. 8. Circumferential strain evolution during process time.

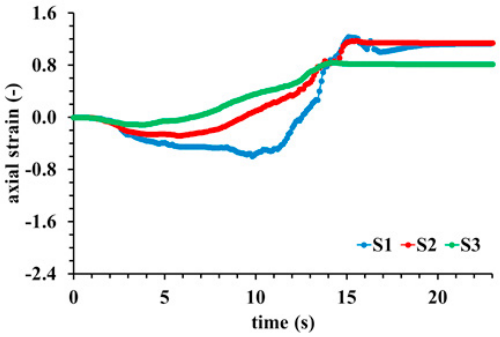

Fig. 9. Axial strain evolution during process time.

The circumferential-axial shear strain (Fig. 11) is similar to the relative sliding along z axis of workpiece radial sections. For the outer (S1) and intermediate layers (S2), initially a negative strain, and then a subsequently positive one, appears. Negative circumferential-axial shear strain is equivalent to a sliding of the material in the opposite direction to the advancement of the rollers. This behavior is called backflow and appears when the roller precedes the sensors: the material interested by the sensors is recalled by the material deformed by the roller, generating a negative displacement of the sensors. Once the roller approaches the sensors, the material flow in the opposite direction disappears and the strain recovery take place. The inner material layers (S3) are not affected by the backflow.

The radial-axial shear strain (Fig. 12) represents the relative displacement of the material in the axial direction. When the rollers deform the material interested by the sensors, inner (S1) and intermediate (S2) material layers are subjected to a relative displacement in the same direction of the roller feed rate, and positive values of radial-axial shear strain appear. After the roller move beyond, strain recovery takes place and outer layers present negative strain.

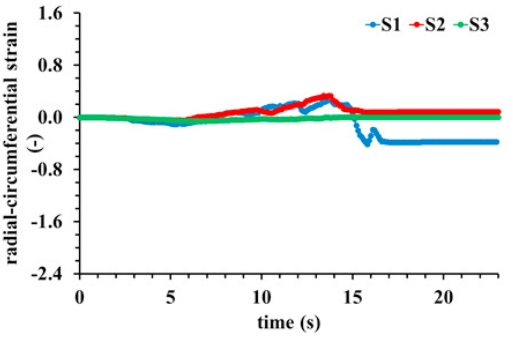

Fig. 10. Radial-circumferential shear strain evolution during process time.

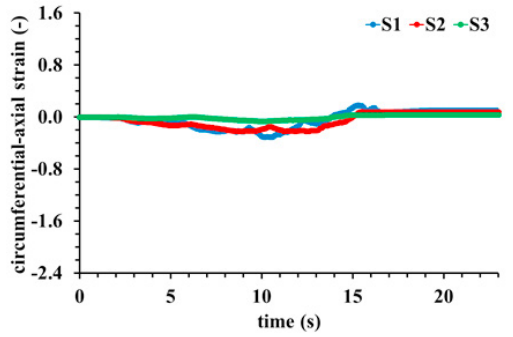

Fig. 11. Circumferential-axial shear strain evolution during process time.

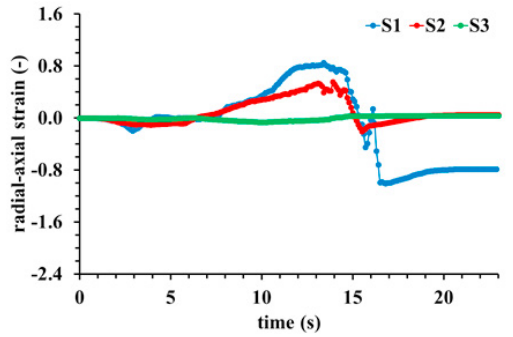

Fig. 12. Radial-axial shear strain evolution during process time.

5. Conclusion

The paper presents the numerical results in terms of stress and strain components evolution during flow forming process. The finite element model representative of process conditions is developed and sensors attached to nodes mesh

are implemented to study the locally deformed material behavior for different workpieces thickness layers.

The results show that:

- The stress components mainly affected by the tool action are normal stress in radial direction (σ_r), normal stress in axial direction (σ_z) and shear stress acting along radial-axial direction (τ_{rz}).
- The hydrostatic pressure assumes positive values (compression) in the material under the roller nose, thanks to the compression effect of normal stress in radial direction (σ_r) and axial direction (σ_z). Once roller moves forward, the hydrostatic pressure reaches negative value due to the decrease of radial compression and the increase of axial tensile load.
- The strain components trend during the process is very complex and characterized by redundant strains that cause the recovery and inversion in strain components evolution.
- Stress and strain components values, as the hydrostatic pressure values, are strongly affected by the location along the workpiece thickness.

References

[1] Wong C, Dean T, Lin J. A review of spinning, shear forming and flow forming processes. Int J Mach Tools Manuf 2003;43:1419–35.
[2] Xu Y, Zhang S, Li P, Yang K, Shan D, Lu Y. 3D rigid–plastic FEM numerical simulation on tube spinning. J Mater Process Technol 2001;113:710–3.
[3] Hua FA, Yang YS, Zhang YN, Guo MH, Guo DY, Tong WH, Hu ZQ. Three-dimensional finite element analysis of tube spinning. J Mater Process Technol 2005;168:68–74.
[4] Mohebbi MS, Akbarzadeh A. Experimental study and FEM analysis of redundant strains in flow forming of tubes. J Mater Process Technol 2010;210:389–95.
[5] Jahazi M, Ebrahimi G. The influence of flow-forming parameters and microstructure on the quality of a D6ac steel. J Mater Process Technol 2000;103:362–6.
[6] Wong CC, Dean TA, Lin J. Incremental forming of solid cylindrical components using flow forming principles. J Mater Process Technol 2004;153–154:60–6.
[7] Wong CC, Lin J, Dean TA. Effects of roller path and geometry on the flow forming of solid cylindrical components. J Mater Process Technol 2005;167:344–53.
[8] Davidson MJ, Balasubramanian K, Tagore GRN. Experimental investigation on flow-forming of AA6061 alloy—A Taguchi approach. J Mater Process Technol 2008;200:283–7.
[9] Ma H, Xu W, Jin BC, Shan D, Nutt SR. Damage evaluation in tube spinnability test with ductile fracture criteria. Int J Mech Sci 2015;100:99–111.
[10] Xu W, Wu H, Ma H, Shan D. Damage evolution and ductile fracture prediction during tube spinning of titanium alloy. Int J Mech Sci 2018;135:226–39.
[11] Bylya OI, Khismatullin T, Blackwell P, Vasin RA. The effect of elasto-plastic properties of materials on their formability by flow forming. J Mater Process Technol 2018;252:34–44.
[12] Novella MF, Ghiotti A, Bruschi S, Capuzzo R. Numerical modeling of AlSi7 tubular components flowformed at elevated temperature. Key Eng Mater 2016;716:753-761.